NJC

ROYAL SOCIETY OF CHEMISTRY

PAPER

View Article Online
View Journal | View Issue

Cite this: *New J. Chem.*, 2026, **50**, 5687

In situ formation of a glassy $MgO/Na_2O–SiO_2$ solid in Scots pine (*Pinus sylvestris* L.) sapwood through a wet-chemistry approach

Edita Garskaite, *[ab] Dane Romar C. Asuigui,[c] Sarah L. Stoll,[c] Lars Hansson[de] and Dick Sandberg[f]

The demand for safe and durable modified-wood products is increasing in the construction sector. In this work, the *in situ* wet-chemistry synthesis of a glassy $MgO/Na_2O–SiO_2$ solid in Scots pine (*Pinus sylvestris* L.) sapwood *via* a two-stage impregnation process using an industrial timber-impregnation autoclave is reported. Magnesium sulphate heptahydrate ($MgSO_4·7H_2O$), a historic fire retardant, and silica-rich sodium silicate ($Na_2O·3.3SiO_2$) solutions were used as the precursors. The degree of wood matrix saturation was controlled by adjusting the $Na_2O·3.3SiO_2$ concentration (0.06 M, 0.3 M and 0.6 M). Wood saturation and density at various stages of the treatment were assessed by X-ray computed tomography (CT), which showed that the internal regions of the wood blocks remained saturated with the solution up to 24 hours post-impregnation. Phase analysis of the coprecipitated powders revealed the formation of amorphous silicates in the $MgO/Na_2O–SiO_2$ system. Thermal analysis showed that the wood treated using a low $Na_2O·3.3SiO_2$ concentration exhibited a behaviour similar to that of the untreated wood and indicated that the thermal stability of Scots pine sapwood can be improved through the incorporation of silicates. This work demonstrates the potential for fabricating hybrid bio-based building materials using water-insoluble solid additives, thereby advancing sustainable construction practices.

Received 6th February 2026,
Accepted 26th February 2026

DOI: 10.1039/d6nj00470a

rsc.li/njc

1. Introduction

Wood is a renewable, bio-based material with excellent structural properties. In recent decades, the possibilities of using wood in buildings have expanded considerably due to its unique combination of characteristics, environmental friendliness, and advancements in mass timber systems that enable faster, safer, and more cost-effective construction.[1,2] Projections indicate a further rise in wood consumption in the coming years.[2,3] Hence, the adoption of circular construction practices, such as enhancing the properties and extending the service life of wood and wood-based products, is becoming essential in preventing the depletion of natural resources and mitigating a wide range of environmental impacts globally.

Wood is a combustible material. Its susceptibility to fire remains one of the key challenges faced by the wood industry[4,5] as fires in structural timber buildings can have devastating consequences and lead to substantial socioeconomic impacts on society.[6,7] To enhance the fire-resistance of wood, various chemical, physical and thermal modifications can be employed, with these processes involving impregnation, surface treatment, or a combination of both.[8–12] Industrially, the impregnation of wood is mainly carried out *via* an autoclave-based process, where chemicals in an aqueous solution are impregnated into the wood using vacuum and pressure in a predefined cycle.

The global flame-retardant chemicals (FRC) market, which is projected to grow from $6.1bn in 2025 to $8bn by the end of 2030, is focusing on alternative-halogen-free additives.[13] Nowadays, the most common inorganic water-soluble preservatives used for flame retardancy contain boron, nitrogen and phosphorus compounds.[14] Boron salts act as fire retardants by promoting char formation and creating a protective glassy layer that insulates the material from heat and oxygen, which

[a] *Institute of Chemistry, Faculty of Chemistry and Geosciences, Vilnius University, Naugarduko 24, LT-03225 Vilnius, Lithuania. E-mail: edita.garskaite@chgf.vu.lt, edita.garskaite@byggtek.lth.se*
[b] *Division of Building Materials, Department of Building and Environmental Technology, Faculty of Engineering, Lund University, Klas Anshelms väg 14, SE-223 63 Lund, Sweden*
[c] *Chemistry Department, Georgetown University, 37th and O Streets NW, Washington, D.C. 20057, USA*
[d] *Wood Science and Engineering, Department of Engineering Sciences and Mathematics, Luleå University of Technology, Forskargatan 1, SE-931 87, Skellefteå, Sweden*
[e] *Department of Ocean Operations and Civil Engineering, Faculty of Engineering, Norwegian University of Science and Technology, Larsgardsvegen 2, 6025 Alesund, Norway*
[f] *Department of Manufacturing and Civil Engineering, Norwegian University of Science and Technology (NTNU), 2821 Gjøvik, Norway*

subsequently inhibits the release of flammable gases,[15] while nitrogen- and phosphorus-containing compounds often act synergistically by offering reduced toxicity and promoting char formation.[16] However, despite their effectiveness as fire retardants, a significant drawback of these ionic compounds is their hygroscopicity and low resistance to leaching.[17] In addition, the concerns regarding boron-based additives due to their potential toxicity highlight the need for safer alternatives.[18,19] Chemicals such as boric acid (H_3BO_3) and sodium tetraborate (Na_3BO_4, borax) were included in the REACH (Registration, Evaluation, Authorisation and Restriction of Chemicals) candidate list of the substances of very high concern (SVHC) as under excessive exposure, these substances can cause skin and respiratory irritation and, in severe cases, even endocrine disruptions.[20] Silicon-based compounds are another type of halogen-free flame retardants. These additives are more effective in the condensed phase, *i.e.* they function by forming a protective char layer, absorbing heat, and releasing water when heated.[21,22] The inorganic silicon systems mainly include soluble silicates, which in daily use are known as waterglass.[12,23] Previous works showed that with glass encapsulation, wood becomes harder, and its strength is increased.[24,25] The mechanical strength of sodium silicate-based materials can be tuned by changing the SiO_2 : Na_2O ratio[26] and thus the mechanical properties of silicate-treated wood.[24,27] In addition to increasing the strength and flame retardancy of materials when used as an additive, sodium silicate solutions are generally considered non-toxic and biodegradable, and they are the most frequently used and cost-effective silicate sources.[25] These attributes make sodium silicates excellent candidates as starting chemicals for the modification and protection of wood.

However, sodium silicates are hygroscopic materials which can leach under elevated moisture conditions.[28–30] To address these issues, several strategies can be employed. One approach is to induce ''fixation'' within the wood matrix through the polymerization of silanol (Si–OH) groups,[23,30–32] which refers to the use of fixatives or binding agents that promote cross-linking,[33] or the application of thermal treatments to ''set'' the additives after vacuum-pressure impregnation.[34] Another method of incorporating silicates into the wood matrix is through a chemical coprecipitation process, which results in wood mineralisation. Previous studies showed that different minerals can be successfully incorporated into the wood matrix, leading to noticeable alteration of wood properties, including calcium carbonate,[35,36] struvite,[37] and brushite ($CaHPO_4{\cdot}2H_2O$).[38] It is often a two-stage treatment process to prepare a material with varying degrees of matrix bulking,[38] which is beneficial for targeted improvements in dimensional stability, mechanical properties and durability.[39]

Silicate minerals are some of the most abundant natural materials. Due to a wide range of properties, these minerals have applications across various sectors including construction,[40,41] geotechnical engineering,[42] environmental remediation,[43] and biomedical fields.[44] The conventional method for producing silicates is solution-based synthesis either through sol–gel or precipitation reactions. Solution-based synthesis has some advantages, as it allows the sintering temperature to be reduced and precise control of the phase homogeneity and morphology. The precursor solutions may be either organic-solvent based or water-based. Chemical processing, which uses water as the solvent, has additional benefits, as it is more environmentally friendly and potentially better suited for industrial processes.[45] In the coprecipitation process, the addition of metal ions to the soluble silicates in water leads to the formation of insoluble metal silicate complexes and subsequent formation of nanoparticles (NPs). The size and shape of these NPs are important parameters for homogeneous filling of the wood matrix and strongly depend on the concentration of reactive species, pH and temperature.[25,46–48] In a basic solution, divalent cations significantly enhance the polymerization of silicic acid (H_4SiO_4) and reduce the solubility of amorphous silica compared with monovalent cation salts;[49–51] this effect decreases in the order of $Mg^{2+} > Ca^{2+} > Li^+ > Na^+ > K^+$.[52] In this work, $MgSO_4{\cdot}7H_2O$ was selected because of the favourable electron-accepting characteristics of Mg^{2+} ions and its use as a fire retardant. When heated, hydrated magnesium sulphate ($MgSO_4$) decomposes endothermically, initially through a multi-step dehydration, and at higher temperatures ($\sim$1100 °C) into magnesium oxide (MgO) and sulfur trioxide (SO_3).[53,54] Furthermore, both $MgSO_4{\cdot}7H_2O$ and MgO are used in cement technology;[47,55–58] this admixture influences the formation of different hydration products and consequently impacts the setting time, strength and durability.[58–60] In cement-based materials, dissolution–precipitation is a fundamental step in the formation of hydration products, and reactivity is governed by the amorphous phase and specific surface area of the material.[40,61–65] Successful incorporation of cementitious materials and ''sealing'' active flame-retardant additives within the wood matrix could open up new horizons for the development of safer, more leach-resistant and more durable hybrid bio-based materials for outdoor and indoor applications.[66,67]

Herein, Scots pine (*Pinus sylvestris* L.) sapwood treatment using aqueous solutions of $MgSO_4{\cdot}7H_2O$ and $Na_2O{\cdot}3.3SiO_2$ was studied. A small-scale industrial timber-impregnation autoclave was used, and a two-stage treatment process was applied to modify the wood. Amorphous $MgO/Na_2O–SiO_2$ solid was formed *via* a coupled salt-dissolution and silicate-coprecipitation process at the wood/salt–fluid interface. The differences in terms of morphology among three concentrations were examined. We found that saturation of the wood cell lumina with the mineral increased with an increasing molar ratio (0.6, 0.2 and 1.4) of Si/(Mg + Na) metals in the precursor solutions. CT was used to monitor the wood matrix saturation during the different treatment steps, which showed that the internal regions of the wood blocks, treated by all routes, remained saturated up to 24 hours post-impregnation. The thermal stability of the mineralised wood was also evaluated. We observed that under the different concentrations, the thermal stability of the mineralised wood was comparable with that of the untreated wood. In addition, the evolution of the mixed-metal silicate powder is also reported and discussed. This relatively simple treatment of wood using silicates could be easily implemented for upscaling and applied to other bio-based materials. The results suggest that the

incorporation of three-component silicates into the wood matrix has potential for the development of environmentally friendly wood-based materials with water-insoluble solid additives.

2. Experimental

2.1. Solutions, wood samples and treatment of wood

Sodium silicate solution ($Na_2O{\cdot}(SiO_2)_x{\cdot}xH_2O$), 26.1% silica ($SiO_2$), 8.1% sodium oxide ($Na_2O$, Technical grade, VWR Chemicals) and magnesium sulphate heptahydrate ($MgSO_4{\cdot}7H_2O$, $\geq$99.5%, ACS, Reag. Ph Eur, Merck) were used as precursor materials. In the aqueous sodium silicate solution, a molar ratio of SiO_2/Na_2O corresponds to 3.31. In the following, this solution is designated as $Na_2O{\cdot}3.3SiO_2$. Three $Na_2O{\cdot}3.3SiO_2$ solutions of 1%, 5% and 10% (by volume) were prepared, and the SiO_2 and Na_2O concentration in these final solutions was estimated to be 0.06 M, 0.28 M and 0.56 M, respectively. 0.05 M $MgSO_4{\cdot}7H_2O$ solution was prepared by dissolving 12.325 g of $MgSO_4{\cdot}7H_2O$ in 1 L of distilled H_2O. The molar ratio of Si/(Mg + Na) metals in the precursor solutions was 0.6, 0.2, and 1.4.

Specimens of Scots pine (*Pinus sylvestris* L.) sapwood having sizes of approximately 10 × 10 × 2 cm and 5 × 2 × 2 cm (tangential (T) × longitudinal (L) × radial (R)) were cut from sawn timber obtained from northern Sweden (Martinsons Trä AB). Specimens were dried in an oven at 103 °C for 48 h (only those that were used to estimate moisture content) and then conditioned in a climate chamber at 20 °C and 65% relative humidity (RH) for 20 days. For the larger specimens, the oven-drying step was omitted. The specimens were weighed before and after the conditioning, and the moisture content (MC) of the samples after conditioning was estimated to be approximately 11.3%. Circular impregnation was used for wood block treatment. Conditioned wood specimens were submerged in the 0.05 M $MgSO_4{\cdot}7H_2O$ solution and subsequently treated by the vacuum-pressure technique using an MAVEB impregnation tube (autoclave). The specimens were kept under vacuum (−50 kPa) for 30 minutes and then for 1 h at a pressure of 1500 kPa. After the vacuum-pressure treatment, the specimens were further kept submerged for 1 h in the solution to allow its maximum diffusion into the wood. Afterwards, the treated specimens (n = 3 for each batch) were dried at 60 °C (80% fan for 24 h) and then additionally treated by the vacuum-pressure technique. 0.06 M, 0.28 M and 0.56 M $Na_2O{\cdot}3.3SiO_2$ solutions were used for cycle-II treatment. The same procedure was performed to additionally impregnate the wood samples. The samples that were impregnated and removed from the autoclave were then conditioned at room temperature under uncontrolled air relative humidity for 30 days.

2.2. Synthesis of MgO–Na_2O–SiO_2 powders

0.05 M $MgSO_4{\cdot}7H_2O$ and 0.06 M, 0.28 M or 0.56 M $Na_2O{\cdot}3.3SiO_2$ solutions were mixed in a 1 : 1 volume in separate microcentrifuge tubes, and 2000 μL of each solution was used. The obtained colloidal suspensions were then centrifuged, decanted and dried at room temperature. The pH of the solutions was checked using pH slips (VWR). The solubility of the Mg–(Na–O–Si) material was determined by washing the coprecipitated powders three times with 2000 μL of demineralised water (BRENNTAG Nordic AB, Malmö, Sweden) with intermediate sonication for 10 min (temperature 4 °C) at 12 000 rpm using a Micro Star 17R microcentrifuge (VWR).

In the following, the Mg–(Na–O–Si)-modified wood samples and coprecipitated powders are designated according to the molar ratio of Si to Mg and Na in the initial solutions, *i.e.* Si/(Mg + Na) = 0.6, 0.2 and 1.4.

2.3. Characterisation

Light microscopy was performed on Olympus DSX1000 digital stereomicroscope coupled with a DSX10-SXLOB Plan 10x/0.20 co/0/OFN22 WD41.1 objective lens, and 2D and 3D images were acquired in a darkfield mixed illumination mode, at the Wood Science and Engineering instrument infrastructure at the Luleå University of Technology (LTU), Skellefteå, Sweden. The morphological features of the untreated and mineralised wood were evaluated using a field emission scanning electron microscope (FE-SEM, SU70, Hitachi) at the facilities of the Institute of Chemistry of Vilnius University (VU), Lithuania. Secondary electron imaging was performed at an electron beam acceleration voltage of 10.0 kV. Infrared spectra (IR) were recorded using a Fourier transform infrared (FT-IR) spectrometer (Frontier FT-IR, Perkin Elmer; ZnSe/Diamond ATR crystal, DTGS detector, 4000–600 cm^{-1}, 4 scans), at the Wood Science and Engineering instrument infrastructure at LTU. Thermogravimetry (TG), derivative thermogravimetry (DTG) and differential scanning calorimetry (DSC) were performed using a PerkinElmer STA 6000 Simultaneous Thermal Analyzer. Dried samples of ∼5–10 mg were heated from 25 °C to 900 °C at a heating rate of 10 °C min^{-1} in dry flowing air (20 mL min^{-1}), at the Institute of Chemistry infrastructure at VU. The thermal behaviour of the mixed-metal silicate dried gels was evaluated by TG using a PerkinElmer TGA 4000 instrument. The weight of the specimens was about 5 mg, which were heated from 30 °C to 820 °C at a constant rate of 10 °C min^{-1}, with nitrogen as the purge gas (flow supply 2 bar), at the Wood Science and Engineering instrument infrastructure at LTU. High-resolution transmission electron microscopy (HR-TEM) analysis was performed on a JEOL JEM-2100F field electron gun (FEG) TEM instrument operated at 200 kV at the Advanced Imaging and Microscopy Lab at the University of Maryland, USA. The formed Mg–Na–O–Si precipitate was washed three times with deionised water and centrifuged, and the samples were prepared for TEM measurements by drop casting precipitated solutions on carbon-coated copper TEM grids. To estimate the average particle size of the coprecipitated solid, TEM images were processed using ImageJ software. X-ray powder diffraction (XRD) patters were obtained using a Rigaku, Ultima IV X-ray diffractometer with Cu-Kα radiation at 40 kV and 30 mA and a D/teX silicon strip detector (2θ = 15°–70°, 0.02 ss, 1° min^{-1}) at the facilities of the Institute of Chemistry, Georgetown University, USA. The elemental distribution of Mg–(Na–O–Si) powders that were washed three times with deionised water and dried at room temperature was studied using a Hitachi TM3000 Tabletop SEM (which

features backscattered-electron (BSE) detector) equipped with an energy dispersive X-ray spectrometer (EDS). The spectrometer was controlled by the INCA software (Oxford Instruments), at the Institute of Chemistry of VU. Backscattered electron detector images were acquired under the electron beam acceleration voltage of 15 kV. An X-ray acquisition time of 590 s was used to obtain the EDS spectra and the elemental mapping images (number of independent measurements (n) = 3, resolution 512 × 384 pixels, image width 235.8 μm).

2.5. X-ray computed tomography (CT)

A Siemens Somatom Emotion Duo medical CT-scanner with a field of view of 500 × 500 mm^2 represented in a grayscale 512 × 512 pixel image, which gave a resolution of 0.98 mm, was used to evaluate the density of the wood blocks as well as their saturation with the impregnating solutions. A beam energy level of 80, 90 and 130 kV was used to scan the specimens (a total of 100 scans with a resolution of 1 mm over a total length of 10 cm). MATLAB software was used to process the 2D images of the wood blocks. The principle of CT scanning is also presented elsewhere.[68,69]

3. Results and discussion

3.1. Morphology of treated wood

To evaluate wood matrix saturation and silicate mineral distribution, light microscopy was used. A micrograph of unmodified wood in cross-section (Fig. 1a) reveals the microscopic structure of the wood matrix, showing distinct regions of earlywood (less dense regions with larger lumina), latewood (denser regions with smaller lumina), intercellular resin canals, and ray cells.[70] The silicate mineral-modified wood exhibited a distinctively different morphology (Fig. 1b–d). The examination of the specimens revealed that wood matrix saturation was strongly influenced by the Mg-to-sodium silicate ratio. The combination of 0.05 M $MgSO_4{\cdot}7H_2O$ and 0.56 M $Na_2O{\cdot}3.3SiO_2$ solutions produced the highest degree of lumina saturation, albeit with a relatively random distribution of filled lumina (Fig. 1d). This can be attributed to the diffusion of the solution in the wood matrix and heterogeneous coprecipitation of the mineral at the liquid–solid interface. Furthermore, the inherent variability of the wood structure and the drying conditions of the treated wood, both of which influence solute transport and reaction dynamics, most likely also contribute to the random lumina filling.

Differences in the surface coverage of the treated wood blocks were also observed. The use of 0.06 M $Na_2O{\cdot}3.3SiO_2$ solution during the second impregnation cycle resulted in the formation of a finely homogeneous silicate layer covering the entire wood block surface (Fig. S1). By contrast, solutions of higher concentration, corresponding to Si/(Mg + Na) ratios of 0.2 and 1.4, appeared to induce more extensive coprecipitation of silicate mineral, leading to less homogeneous surface coverage with solid inorganic deposits (data not presented). The variations in wood-matrix saturation and the decrease in surface coverage homogeneity can be ascribed to the different amounts of ionic species available to participate in the ion-exchange and silicate polymerisation reactions, as the agglomeration of silicate particles is concentration dependent.[48] In addition, the drying conditions for the treated wood and evaporation of solvent (water) from the wood matrix are also expected to influence the formation of solid material and its rate of sedimentation on the internal walls of the cell lumina and likely on the wood surface. Moreover, the increased accumulation of coprecipitated silicate mineral on the side of the wood block, as shown in Fig. 1c, can be attributed to the rapid reactivity of Si–O species with Mg^{2+} ions upon contact with the Mg-treated wood. A higher concentration of ionic species accelerates the coprecipitation reaction, leading to faster mineral deposition and more pronounced localised accumulation along the wood block surface. This suggests that the kinetics of mineral formation are strongly dependent on both the concentration and distribution of reactive ionic species within the wood matrix. The kinetics of silica precipitation in the presence of alkali and alkaline earth cations have been reported previously, indicating that coprecipitation phenomena are governed by multiple variables.[71,72] It is also worth noting that relevant studies elucidating the formation of the mineral $CaHPO_4{\cdot}2H_2O$ within the wood matrix have been reported.[38] *In situ* XRD measurements showed that precipitation of $CaHPO_4{\cdot}2H_2O$, which crystallises in the monoclinic space group *Ia*, was observed within a few seconds after the solutions were mixed, while the main $\bar{1}12$ diffraction peak of the crystalline phase was detected approximately 8 min after the start of the precipitation experiment, confirming the high

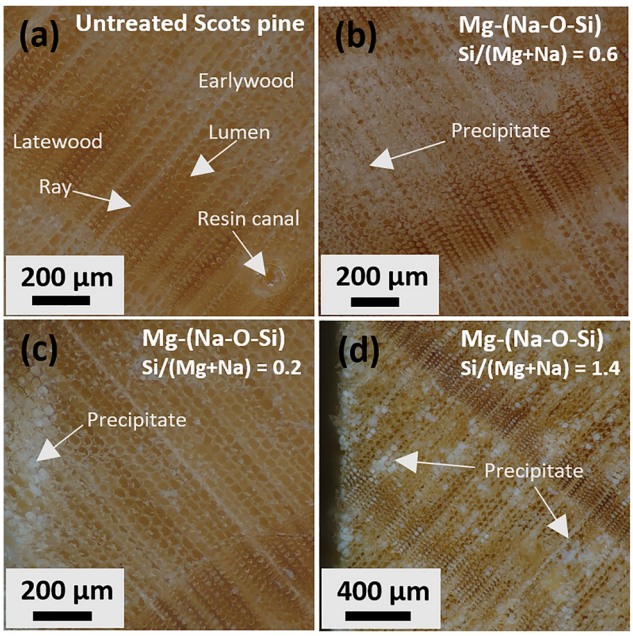

Fig. 1 Photomicrographs of the cross-section of the surface of (a) unmodified and (b)–(d) Mg–(Na–O–Si)-modified Scots pine sapwood (specimens of 2 × 1.5 × 2 cm). The top surface layer of the wood blocks used for imaging was cut with a microtome to enhance the smoothness of the surface and the visualisation of the wood structure.

reactivity of these ionic species in aqueous media and the complexity of crystalline mineral formation within the wood–organic composite matrix.

To further investigate the morphological features of the mineralised wood, FE-SEM analysis was conducted. The FE-SEM images of the modified wood correlate well with the optical microscopy observations; the SEM data confirm that the voids within the treated wood are filled to varying degrees with solid material and that matrix saturation is dependent on the solution concentration. Representative FE-SEM images of the silicate-modified wood with Si/(Mg + Na) ratios of 0.6 and 1.4 (blocks cut in cross-section) are shown in Fig. 2. In the case of silicate-treated wood at an Si/(Mg + Na) molar ratio of 0.6, coprecipitated silicate particles can be clearly observed on the mineralised cell walls (Fig. 2a and b). As previously noted, the highest degree of lumina saturation with mineral was achieved in the wood samples treated with the most concentrated solutions, *i.e.* at an Si/(Mg + Na) ratio of 1.4 (Fig. 2c and d). SEM analysis confirmed that complete filling of the lumina was location dependent.

3.2. Structure evaluation of treated wood

The chemical composition of the modified wood was determined by FTIR spectroscopy. The IR spectra of the untreated and modified wood are shown in Fig. 3 (only the region of 1800–600 cm^{-1} is presented). The spectrum of the unmodified wood exhibited characteristic bands corresponding to the principal chemical constituents of wood, *i.e.* cellulose, hemicellulose and lignin, in agreement with our previous works.[24,73] A comparison of the IR spectra of the modified and unmodified wood revealed different absorbance bands within four regions, namely 2940–2840 cm^{-1}, 1750–1540 cm^{-1}, 1300–1200 cm^{-1} and 830–730 cm^{-1}.

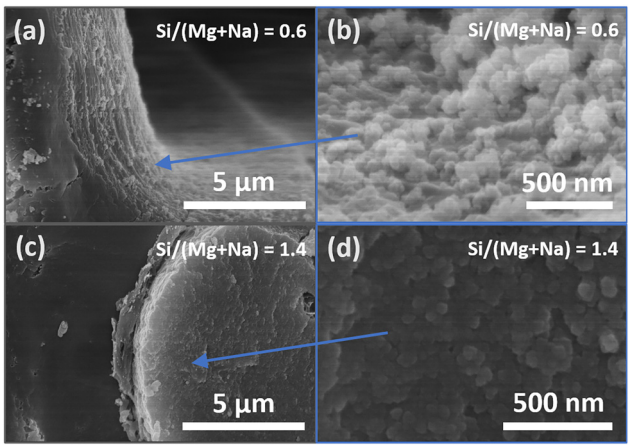

Fig. 2 FE-SEM images of the cross-section of Mg–(Na–O–Si)-modified Scots pine wood: (a) and (b) Si/(Mg + Na) = 0.6 and (c) and (d) Si/(Mg + Na) = 1.4. The high magnification images in (b) and (d) show the morphology of the actual mineral coprecipitated within the cell lumina (place of investigation is not specified; arrows indicate the approximate place of examination).

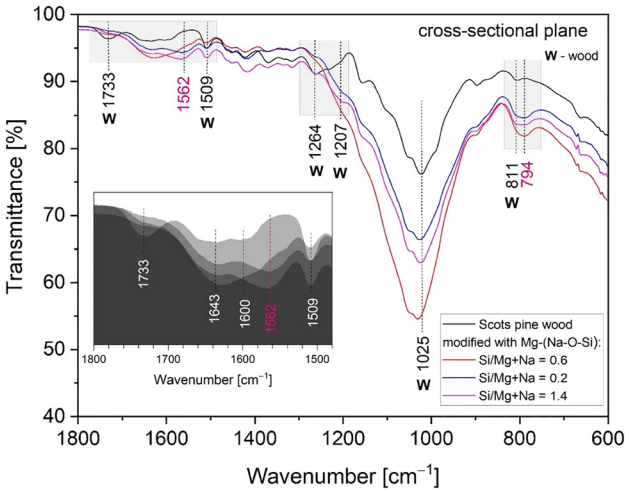

Fig. 3 IR spectra of the untreated and Mg–(Na–O–Si)-modified Scots pine sapwood (region of 1800–600 cm^{-1}). Inset: Expanded region indicating the changes in the wood after modification.

The bands located in the 2940–2840 cm^{-1} region arise from the C–H asymmetric stretching in the methyl and methylene groups of cellulose and hemicellulose.[24,74] Hemicellulose is the most hygroscopic fraction of the wood. The observed changes in the intensities of these bands (maxima at 2926 cm^{-1} and 2880 cm^{-1}) indicate partial removal of hemicellulose as a result of alkaline wood treatment.

Several components give IR absorption bands in the 1750–1500 cm^{-1} region. The bands at 1509 cm^{-1} and approximately 1600 cm^{-1} are characteristic of the C=C stretching vibrations of the aromatic ring in lignin. No positional shifts or changes in the band shape were observed at 1509 cm^{-1} after modification. The IR spectra of the modified wood exhibited a distinctive broad band at approximately 1562 cm^{-1}, which might be attributed to the asymmetric stretching of carboxylate (COO^-) anions, although further validation is required. In addition, C=O stretching frequencies of unconjugated ketones, carbonyls, aldehydes, and ester groups appear at 1740–1710 cm^{-1} (maximum at 1733 cm^{-1}).[75,76] The intensity of this broad band decreased markedly after the modification. Conversely, the band located at 1633 cm^{-1} increased in intensity in the modified wood, which can be ascribed to the attachment of water molecules to the C=O groups of the aromatic structures of the wood constituents (galactoglucomannans, xylans and the less soluble glucomannans).[24]

In the 1300–1200 cm^{-1} region for the unmodified wood, three broad bands with maxima at 1263, 1231 and 1207 cm^{-1} were prominent. The band at 1263 cm^{-1} originates from the ν(C–O) stretching vibrations in lignin, the band present at 1231 cm^{-1} corresponds to alkyl–aryl–ether bonds and lactones, and that at 1207 cm^{-1} to O–H bending in cellulose.[24,76,77] Significant changes in the intensities of these bands were observed after modification, where the intensity of the band at 1263 cm^{-1} decreased, while those at 1236 and 1207 cm^{-1} increased. This also indicates that the alkali treatment partially removes the hemicellulose, thereby increasing the accessibility of O–H groups to water.[24]

The fingerprint region is dominated by bands approximately at 1050–900 cm^{-1}, which are associated with various polysaccharide vibrations.[78] Cellulose exhibits vibrations between 1100 and 900 cm^{-1}. After the modification, slight shifts in the positions and intensities of the main bands were observed, which may be attributed to the presence of coprecipitated silicates.[79] The band at 811 cm^{-1} for the unmodified wood is due to C–H out-of-plane bending vibrations in lignin. Following modification, this band overlapped with a new band at 794 cm^{-1}, which could be assigned to Si–O–Si species.[24,79]

3.3. Studies of wood matrix saturation using X-ray computed tomography (CT)

To estimate the saturation of the wood matrix with the impregnating solution, CT was performed. CT is a useful non-destructive method for measuring the distribution of moisture content (MC) in wood.[80,81] Three wood blocks were studied for the same chemical modification (Si/(Mg + Na) ratios of 0.6, 0.2 and 1.4). Four CT scans were performed on each wood block: (i) before treatment (untreated wood block), (ii) after the cycle-1 impregnation with $MgSO_4$ solution, (iii) after the cycle-2 impregnation with sodium metasilicate solution, and (iv) after drying of the silicate-modified wood blocks at room temperature for 30 days.

Representative segmented CT images of the unmodified Scots pine and wood modified with solutions at Si/Mg = 0.8, with scanning performed at 80 keV, are presented in Fig. 4. The CT images show the cross-sectional views of the same wood block with dimensions of 10 × 10 × 2 cm. One can observe that after cycle-1 impregnation, and subsequent drying at 60 °C for 12 h, the wood blocks retain a significant amount of moisture. This appears as brighter regions within the centre of the wood block (Fig. 4b), confirming complete diffusion of the solutions into the wood block. This is consistent with our previous EDS analysis data of $MgSO_4$ solution-impregnated and dried wood, which showed the presence of Mg and S elements (data not presented), thereby confirming full matrix saturation. However, it should be noted that some specimens developed small cracks after treatment and oven-drying at 60 °C. These are so-called 'shrinkage cracks', which occur due to an uneven moisture content distribution within the wood during the moisture removal process through evaporation. Generally, the factors that affect wood drying can be divided into two groups, *i.e.* external and internal. External factors include temperature, humidity and air circulation velocity, while internal factors comprise wood species, structural characteristics (wood grain direction and heartwood *vs.* sapwood), wood thickness, and wood MC.[82–84] Although some cracks are harmless, the drying conditions (temperature, exposure time, and placement of samples in the drying chamber) should still be optimised to preserve the wood structure and to minimise treatment-induced defects that may negatively influence material properties, such as the strength of components and structures.[85] From a technical point of view, this is particularly important when fabricating larger wood samples.

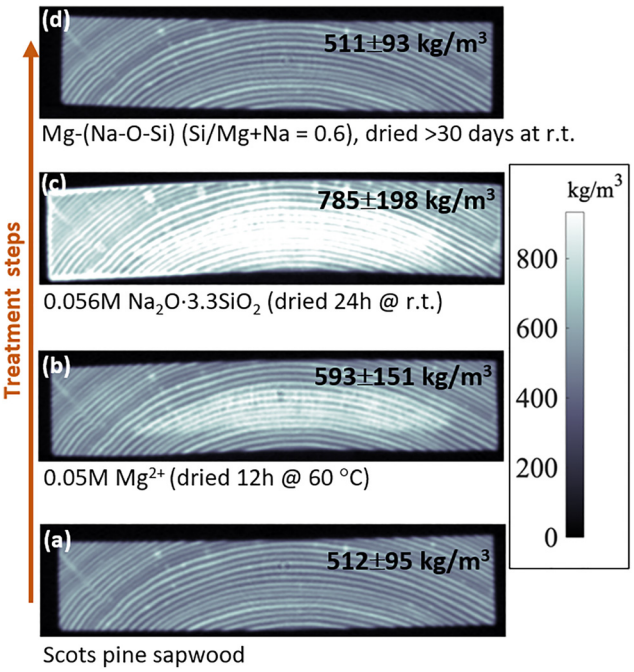

Fig. 4 Segmented CT images showing the macroscopic internal structure of the Scots pine sapwood blocks from a treatment, and lighter regions within the centre of wood block indicating the presence of moisture (original size of wood blocks = 10 × 10 × 2 cm): (a) untreated wood and the same wood block, (b) after 1st impregnation cycle, treated with 0.05 M $MgSO_4$ and dried for 12 h at 60 °C, (c) after 2nd impregnation cycle, treated with 0.056 M $Na_2O{\cdot}3.3SiO_3$ and dried at room temperature for 24 h, and (d) modified and dried wood (Si/(Mg + Na) = 0.6) at room temperature for 30 days. (Reconstructed images are from the middle of the block, with the scanning performed at 80 keV).

The CT image of the wood block after the cycle-2 impregnation with sodium silicate solution and subsequent drying for 24 h at room temperature is shown in Fig. 4c. The MC distribution across the cross-section is clearly distinguishable, with a higher content in the centre of the block. This indicates that coprecipitation of silicate minerals can proceed throughout the wood. Further drying at room temperature for 30 days resulted in a homogeneous cross-sectional morphology (Fig. 4d). As the sorption of solution by wood proceeded to the core of the block, the formation of mixed-metal silicates within the matrix is expected. The precipitation of silicates was further confirmed by calculating the density values. The average density values for the Si/(Mg + Na) = 0.6 system were 512 ± 95 kg cm^{-3} (untreated wood), 593 ± 151 kg cm^{-3} (after cycle-1), 785 ± 198 kg cm^{-3} (after cycle-2) and 511 ± 93 kg cm^{-3} (modified and dried wood). The density values are presented in Table S1. Additional scans at beam energies of 110 and 130 keV were also performed. Nevertheless, only negligible changes in density values were observed for the specimens from the same batch of the same modification treatment (Table S1). CT analysis also revealed a slight decrease in mass following modification (data not presented), which may be attributed to the removal of non-structural chemical compounds (extractives present in wood) during the alkaline treatment, as well as the intrinsic density of the silicate mineral incorporated into the matrix.

Ultimately, the CT studies revealed complete saturation of the wood matrix, which is essential for producing uniformly treated wood. However, one may note that the permeability of different timber species to preservative-medium penetration is closely related to the anatomical differences in the wood structure. This factor should be taken into consideration when evaluating treatments for other wood species.

3.4. Evolution of $MgO/Na_2O–SiO_2$ solids

Understanding particle formation in the reaction medium is essential for elucidating solid intercalation into the wood matrix and the properties of the resulting material. To assess the structure of the coprecipitated silicates, HR-TEM analysis was performed. The TEM images of the obtained coprecipitated powders and those washed with distilled water from solutions with an Si/(Mg + Na) molar ratio of 0.6 and 1.4 are shown in Fig. 5. At an Si/(Mg + Na) molar ratio of 0.6, aggregated clusters were observed, and the emerging silica-based particles possess an amorphous structure (Fig. 4a and b). By contrast, the precipitates from more concentrated solutions displayed a distinct nanostructure (Fig. 4c and d), in which amorphous particles were randomly embedded within a continuous gel-like phase. The average particle size was calculated to be 45.4 ± 8.7 nm (n = 23).

Gelation (condensation of monomers) of the sodium silicate solution in aqueous media was induced by Mg^{2+} ions. Alkali-soluble metasilicate is known to react with Mg^{2+} ions to form insoluble magnesium silicates. Particle evolution is Na/Si molar ratio dependent, and concentration, pH and temperature play significant roles in nucleation.[48,86] The higher sodium metasilicate content in the initial solution resulted in different rates of monomeric silica consumption, which in turn governed the nucleation, growth and agglomeration of particles in aqueous media. It has been reported that Na^+ ions in sodium metasilicate solution act as SiO_2 surface-stabilising agents, *i.e.* Na^+ ions are strongly adsorbed onto silanol groups, expressed as Si–ONa.[25] The rate of aggregate growth strongly depends on the presence of polyvalent cations. Colloidal silica in aqueous media is highly reactive, and the addition of $MgSO_4$ solution disturbs the ionic balance *via* ion exchange. Magnesium ions, owing to their higher charge density, exert a more pronounced destabilising effect than monovalent ions. When Mg^{2+} ions are introduced into the system, gelling immediately proceeds, as added polyvalent ions function as a SiO_2 surface modification agents, leading to the formation of different Si–O–(Mg–O)/Na species.

Colloidal components in diluted sodium metasilicate contain more monomer in solution.[87] At low silicate concentrations, condensation produced homogeneously clustered particles, while supersaturation at higher concentrations favoured heterogeneous morphologies. These observations confirm that the initial solution conditions strongly influence particle growth, packing and silicate phase formation within the $MgO–Na_2O–SiO_2$ system.

From a wood modification perspective, particle size is critical for diffusion into cell-wall cavities. This implies that lower-concentration solutions may facilitate greater primary particle penetration into the wood matrix, leading to more uniform filling of the cell-wall network. Therefore, factors governing silica polymerisation must be carefully considered to achieve a homogeneous distribution of material with the desired phase and composition within the wood structure.

The elemental composition of the coprecipitate was evaluated using SEM/EDS analysis (Fig. 6). The SEM-BSE image of agglomerated powders obtained from solutions with an Si/(Mg + Na) molar ratio of 1.4 (Fig. 6a) and washed with demineralised water shows no variation in contrast, indicating a homogeneous elemental distribution. The EDS analysis confirmed the presence of C, O, Na, Al, Mg, and Si (Fig. 6b). The detected Al originated from the sample holder. No presence of S element was detected, indicating that sulphate (SO_4^{2-}) ions had been washed out from the co-precipitated powders. This further suggests that migration of spectator ions, SO_4^{2-} and Na^+ from the wood matrix is likely to occur under elevated moisture conditions, even though these ions were successfully incorporated into the entire wood block during impregnation cycle-I. Nevertheless, forming a composite of silicates with other minerals, such as sulphates, hydroxides and carbonate, could lead to the development of cementitious materials. This, in turn, indicates that adjustments to both the mineral synthesis process and wood treatment method should be considered to enable the modification of wood with leach-resistant cement-based materials.[88]

The EDS mapping images of the individual elements in the analysed powder sample (Fig. 6c) further demonstrated the homogeneous distribution of Mg, Na, O and Si within the agglomerate, indicating the formation of a three-component solid coprecipitate under the present experimental conditions. Leachate studies on Scots pine treated with H_3BO_3, zinc chloride ($ZnCl_2$), aluminium chloride ($AlCl_3$), and a combination of these chemicals with silica gel have been reported by Altun *et al.* They showed that silica gel treatment prevented leaching of the active chemicals from Scots pine cell walls and lumina.[89] Specifically, the leaching of the active chemical, H_3BO_3, from Scots pine treated with H_3BO_3 and silica gel was 1.5-times lower

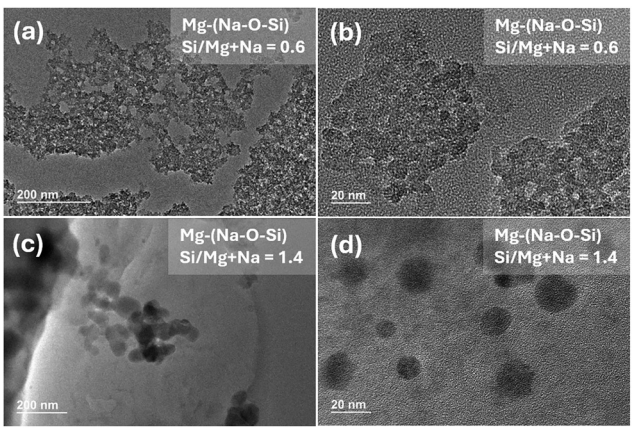

Fig. 5 HR-TEM images showing the particles evolved in the $MgO–Na_2O–SiO_2$ system: (a) and (b) Si/(Mg + Na) = 0.6 and (c) and (d) Si/(Mg + Na) = 1.4.

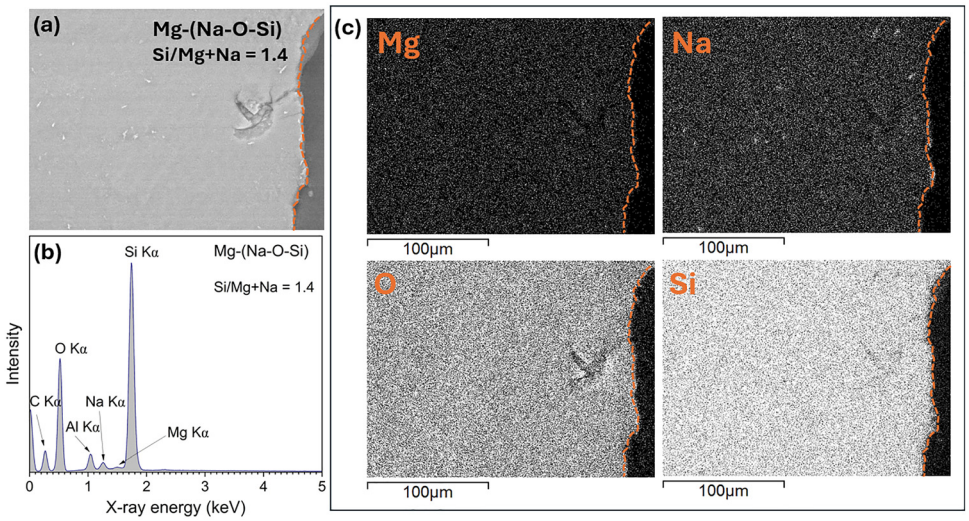

Fig. 6 SEM and EDS backscattered images of the powders formed from the solutions of Si/(Mg + Na) = 1.4 showing (a) morphology of the coprecipitated and washed powders, (b) EDS sum spectrum with the elements detected, and (c) EDS elemental mapping of Mg, Na, O and Si. The orange dotted lines in (a) and (c) show the corner side of the agglomerate.

than that of the specimens treated with H_3BO_3 alone. Furthermore, we conducted studies (unpublished data) in which calcium phosphate-mineralised wood was exposed to natural weather conditions (the data are available in a report published elsewhere[90]). SEM/EDS analysis showed that calcium phosphate, after three months of exposure to natural weather conditions, remained present within the Scots pine wood matrix. This suggests that altering the properties of wood by incorporating minerals into the wood structure may be an attractive approach to produce materials suitable for exterior applications or for use under conditions where the MC exceeds sustainable limits without deterioration.

The XRD patterns of the Mg–(Na–O–Si) powders, washed after coprecipitation and dried at room temperature (20 °C–25 °C), are presented in Fig. 7. The absence of Bragg reflections confirms that coprecipitates are amorphous solids and agrees with the literature.[86] The TG and DTG curves of the Mg–(Na–O–Si) powders (Si/(Mg + Na) = 0.6) are shown in Fig. 7 (inset). The weight loss of ~13% up to 120 °C can be attributed to the removal of free and bound water. The TG curve shows no weight-loss stages in the range of 200 °C–400 °C or above 420 °C, which suggests that no hydrates are formed in the system. The coprecipitated powders from the other systems (Si/(Mg + Na) = 0.2 and 1.4) exhibited similar thermal behaviour. However, absorbed water content differed, where the highest amount of released water during drying at up to 130 °C was observed for the powder of the Si/(Mg + Na) = 0.2 system (data not presented). This implied the different reactivity of silicate or polysilicate anions, arising from the surface silanol groups, and subsequently the formation of distinct silicate structures, as the molar ratio SiO_2/Na_2O and water content influence the structure of the silicates formed.[91,92]

The IR spectra of the Mg–(Na–O–Si) powders dried at room temperature and annealed at 810 °C are presented in Fig. 8. The powders dried at room temperature (Fig. 8a) exhibit bands

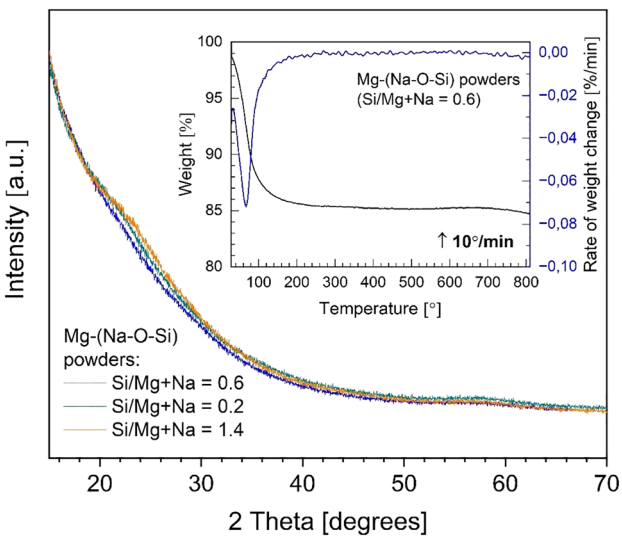

Fig. 7 XRD patterns of the coprecipitated Mg–(Na–O–Si) powders washed with distilled water and dried at room temperature. Inset: TG/DTG curves of the representative Mg–(Na–O–Si) gel (Si/(Mg + Na) = 0.6) washed and dried at room temperature for 10 days.

characteristic of silicate groups. The broad absorption bands in the 900–1100 cm^{-1} region are attributed to the stretching vibrations of the Si–O–Si bonds. The maximum of this band shifts towards lower wavenumbers with an increasing SiO_2 concentration (1049 cm^{-1}, 1015 cm^{-1} and 1005 cm^{-1} for the systems with Si/(Mg + Na) = 0.6, 0.2 and 1.4, respectively). This slight shift indicates the formation of different mixed-metal silicates, as the position of the Si–O–Si bands depends on the Si/metal molar ratio within the silicate. A shift relative to that of similar glasses reported in previous studies is observed.[79,93,94] The diversity of silicates can largely be attributed to the isomorphous substitution of one cation by another. Since the

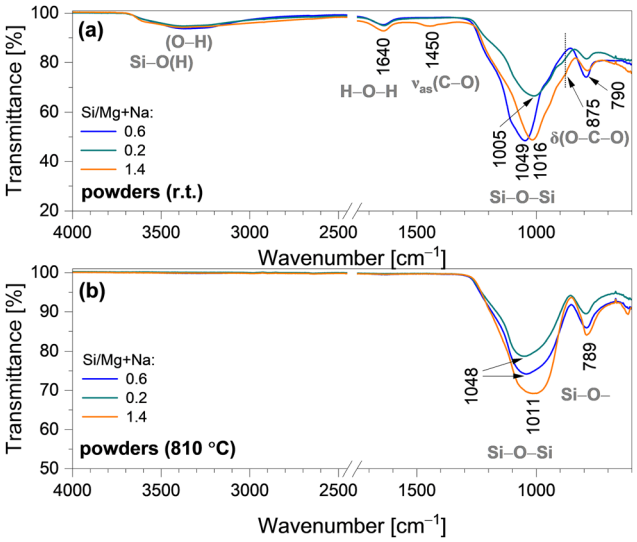

Fig. 8 IR spectra of the Mg–(Na–O–Si) gels: (a) as-coprecipitated and dried at room temperature (r. t.) for 10 days and (b) after annealing at 810 °C.

Mg^{2+} ion is a stronger Lewis acid than the Na^{+} ion, it is more likely to coordinate with Si–O^{-} groups, *i.e.* Mg^{2+} exhibits greater affinity for Si–O than Na^{+}.[95]

Another broad, but less intense, band corresponding to Si–O–Si vibrations was observed in the 795–785 cm^{-1} region.[96] This is in good agreement with the wood-silicate spectra discussed above. The IR spectra of the powders also exhibited a band at 1640 cm^{-1}, which was assigned to the hydroxyl (O–H) vibrations of water molecules. In addition, a broad band in the 3600–3400 cm^{-1} region was observed, corresponding to the stretching vibrations of the O–H group; silanol Si–O(H) groups may also contribute to absorption in this region.[97] Interestingly, the IR spectrum of the powders obtained from the highest concentration solution (Si/(Mg + Na) = 1.4) displayed a broad band at ~1450 cm^{-1}, which can be attributed to the absorption of CO_2 or carbonate ions (CO_3^{2-}).[98] A weak shoulder at 875 cm^{-1} was also present in the systems of Si/(Mg + Na) = 0.2 and 1.4, which is assigned to the O–C–O vibrations of CO_3^{2-} groups.

In the spectra of the powders annealed at 810 °C (Fig. 8b), the bands assigned to H_2O (3600–3400 cm^{-1} and 1640 cm^{-1}) and carbonate groups (1450 cm^{-1}) disappear, indicating that these species are not incorporated in the mineral structure.[98] Again, a small shift in the Si–O band (at around 1011 cm^{-1}) suggests local structural variations in the silicate network. As noted above, the structure of the evolving silicates is a consequence of the successive polymerization, gelation, ageing, drying and heating processes. Nevertheless, to estimate the arrangements, geometries and configurations of Si–O–Si units, further studies, such as solid-state NMR, are required.[99]

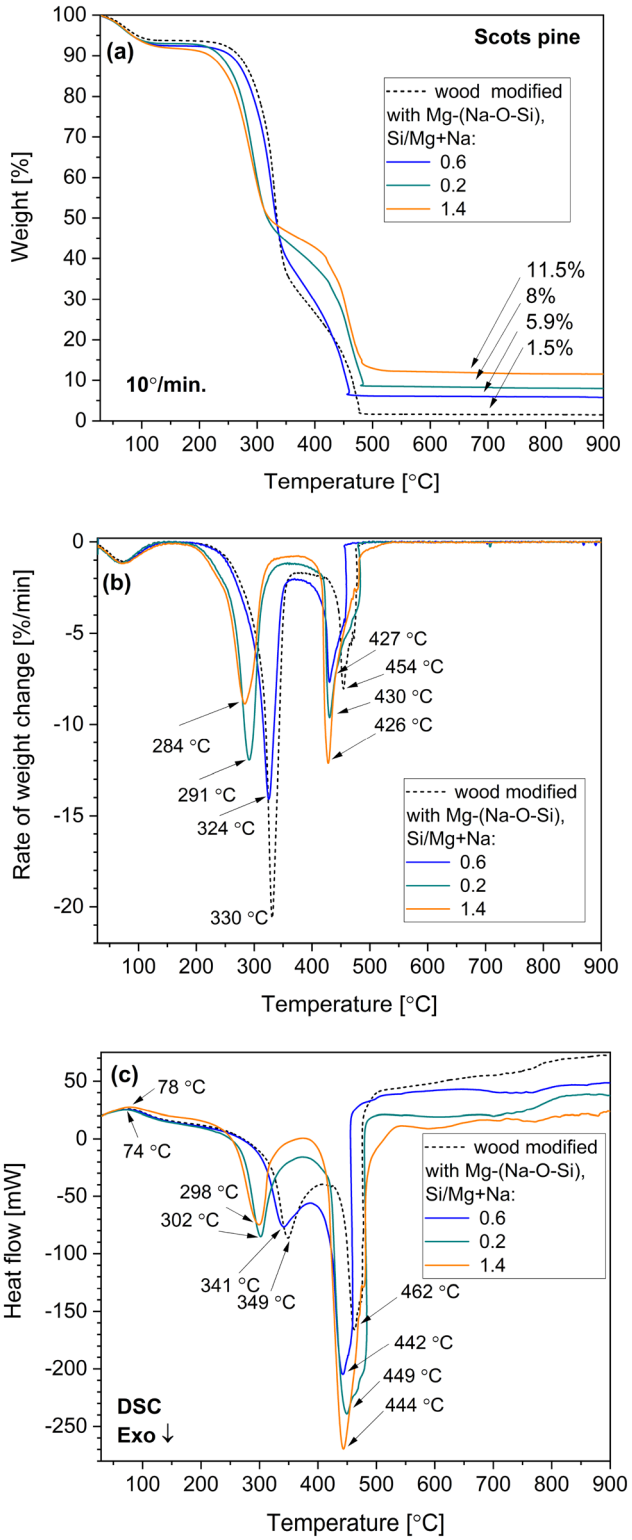

Fig. 9 Thermal behaviour of the unmodified and silicate-treated Scots pine sapwood: (a) TG, (b) DTG and (c) DSC curves.

3.5. Thermal behaviour of silicate-mineralised wood

The thermal behaviour of the unmodified and silicate-treated Scot pine sapwood was evaluated by thermal analysis. The TG/DTG and DSC curves, as presented in Fig. 9, reveal three stages of weight loss, leaving approximately 1.5%–11.5% residue at 470 °C–480 °C. For the untreated wood, an initial weight loss of 5% (Fig. 9a) was observed up to 105 °C, accompanied by a small endothermic peak at 74 °C (Fig. 9c), which was assigned to the

removal of absorbed water. The second and most significant weight loss (60%) occurred between 250 °C and 350 °C (DTG maximum at 330 °C, Fig. 9b), followed by a strong exothermic peak at 349 °C. This weight loss was ascribed to the decomposition of the wood constituents, where hemicellulose, cellulose and lignin are pyrolysed at 200 °C–300 °C, 280 °C–350 °C and 280 °C–650 °C, respectively. This process involves a series of reactions including dehydration, decarboxylation, decarbonylation and fragmentation, accompanied by the release of volatile components, such as CO_2, CO, acetic acid (CH_3COOH), methanol (CH_3OH) and high-boiling-point tar.[24] The third weight loss of 33.5% was observed between 350 °C and 480 °C, corresponding to the further degradation of lignin, which is oxidised to CO_2, CO and H_2O. No mass change was detected above 480 °C, and the residual carbon-rich inorganic fraction accounted for 1.5% of the initial mass.

The wood treated with the Si/(Mg + Na) = 0.6 system exhibited behaviour similar to that of the untreated wood, but with a residual mass of 6% at 470 °C, confirming the successful diffusion of the treatment solutions and coprecipitation of inorganic materials within the wood matrix. In contrast, the wood modified with the Si/(Mg + Na) = 0.2 and Si/(Mg + Na) = 1.4 systems exhibited the first weight loss of 7% and 9%, respectively, up to 130 °C. This was attributed to the larger amounts of absorbed water retained within the silicates precipitated within the wood matrix. Both treatments resulted in a shift of the onset temperatures to lower values and produced a net mass gain after pyrolysis. The second and third weight losses occurred at lower temperatures of approximately 50 °C and 15 °C for the Si/(Mg + Na) = 0.2 and Si/(Mg + Na) = 1.4 systems, respectively, compared with the untreated wood. This behaviour is likely due to the structural changes induced when the wood components interact with the alkaline $Na_2O{\cdot}3.3SiO_2$ solutions, as well as the heat absorbed by the amorphous mineral, which affects the combustibility of the wood components. Despite the comparable events observed in the DSC curves (Fig. 9), the overall results indicate that the decomposition temperature of the wood reinforced with solid of the $MgO–Na_2O–SiO_2$ system can increase to higher temperatures with an increase in the ratio of $MgSO_4{\cdot}7H_2O$ to $Na_2O{\cdot}3.3SiO_2$, thereby enhancing the thermal stability of the composite. The residual masses after pyrolysis were 8.0% and 11.5% for the Si/(Mg + Na) = 0.2 and Si/Mg = 1.4 systems, respectively, correlating with the increase in sodium metasilicate concentration in the initial treatment solutions.

In general, the thermal behaviour of gels (amorphous matrices) strongly depends on their drying conditions. Physically absorbed water is lost at 100 °C–150 °C, while dehydration begins at 200 °C–400 °C and proceeds rapidly by 500 °C–600 °C, at which point the remaining bound water is removed and the gel then forms a stable structure, leading to crystallisation and the formation of different silicate systems. Silicon atoms, tetrahedrally coordinated by oxygen, undergo varying degrees of structural modification and disorganisation due to replacement of the O–H and O^{2-} groups. Depending on the composition (notably the presence of Na^+ and Mg^{2+} ions), different crystalline phases may form at higher temperatures (900 °C–1100 °C). Consequently, the complexity of the phases formed during heating may enable the decomposition products of the silicates to transform into more stable phases, and thus alter the degradation behaviour of wood–silicate composite materials.

To comprehend the thermal degradation and gain a better understanding of the processing–composition–properties relationship, the thermo-chemical properties of the mineralised wood was further elaborated. This includes measurements of the limiting oxygen index (LOI), as well as microscale combustion calorimetry (MCC) and cone calorimetry (CC) tests. A relevant study, where the LOI values of wood treated with a mixture of sodium silicate and nano-TiO_2 mineral were reported by Garskaite *et al.*, demonstrated that the oxygen fraction required to sustain combustion during LOI testing increased with an increasing concentration of the components.[24] In another study, it was shown that an increased concentration of mineral brushite, inorganic filler, within the wood matrix, led to an increase in evolved gas during thermal degradation test.[38] This suggests that inorganic additives in bio-based composite materials play an important role in modulating fire retardancy. In particular, endothermic cooling, flame dilution through the release of non-combustible gases, and char-barrier formation should be carefully considered when designing these inorganic-additive reinforced bio-based materials.

It should also be noted that although the scope of this study has been about the wet-chemistry synthesis of three-component silicates within the wood matrix, there is much still to learn about the produced materials. For example, an evaluation of their mechanical properties would be central to their further study, as these materials are intended for construction applications. In the current work, we did not measure the strength of the Mg–(Na–O–Si)-modified wood. Earlier studies showed that the mechanical strength (for example, indentation-based testing, compressive strength perpendicular/parallel to the fibre, and bending strength in radial and tangential directions) of inorganic-filler reinforced wood are comparable with that of untreated wood.[24,38,100] This motivated us to elucidate the crucial steps in the synthesis process and how to obtain homogeneously mineralised wood with different degrees of matrix saturation.

This study highlights the importance of selecting an appropriate wood treatment procedure to achieve varying degrees of matrix saturation with multicomponent silicates, which influence the resulting wood properties. Furthermore, this work paves the way for continued investigations of wood modifications using diverse cementitious materials and offers potential for the development of hybrid, environmentally sustainable, bio-based building materials.

Conclusions

A non-crystalline $MgO/Na_2O–SiO_2$ solid was successfully synthesised *in situ* within Scots pine sapwood *via* a coupled $MgSO_4$ salt-dissolution and silicate coprecipitation process at the wood/salt–fluid interface. Multiscale characterisation confirmed both the effectiveness of the treatment and the

controllability of mineral incorporation. Optical microscopy and SEM demonstrated that adjusting the sodium silicate concentration resulted in different degrees of wood matrix saturation. X-ray CT showed that internal regions of the wood blocks remained saturated 24 h post-impregnation, highlighting the importance of the wood drying process to obtain homogeneous coprecipitation of minerals. TEM and XRD revealed the amorphous nature of the coprecipitated phase, while EDS verified the presence of Mg, Na, and Si within the powders, confirming the successful incorporation of a water-insoluble three-component silicate within the wood matrix. FTIR spectroscopy further confirmed the integration of silicate into the wood matrix and revealed CO_2/carbonate uptake during processing, which was most pronounced at higher sodium silicate concentrations. The thermal stability of the modified wood was demonstrated to be good, with the potential to be further increased by optimising the amount and structure of incorporated silicate mineral. Overall, the findings demonstrate a controllable wet-chemistry route for engineering mineral-wood composite systems through regulation of solution chemistry and wood treatment procedures. This approach offers potential for further wood modifications using diverse cementitious systems and supports the development of hybrid, environmentally sustainable, bio-based building materials.

Conflicts of interest

There are no conflicts to declare.

Data availability

All data are held in the repositories of the Institute of Chemistry at Vilnius University, the Department of Chemistry of Georgetown University, and the Department of Engineering Sciences and Mathematics at the Luleå University of Technology.

Supplementary information (SI): optical microscope images acquired in 3D and density values calculated from CT images. See DOI: https://doi.org/10.1039/d6nj00470a.

Acknowledgements

This work has been partially supported by the Swedish Research Council FORMAS project ''Utilization of solid inorganic waste from the aquaculture industry as wood reinforcement material for flame retardancy'' (grant no. 2018-01198). Andrius Pakalniškis (the Institute of Chemistry, Vilnius University, Lithuania) is acknowledged for recording the TG/DSC curves. SLS thanks the NSF (CHE-2304974).

References

1 D. Buck, P. Wallentén, M. Sehlstedt-Persson and M. Öhman, *Mater. Des.*, 2023, **230**, 111967.
2 G. Churkina, A. Organschi, C. P. O. Reyer, A. Ruff, K. Vinke, Z. Liu, B. K. Reck, T. E. Graedel and H. J. Schellnhuber, *Nat. Sustain.*, 2020, **3**, 269–276.
3 B. D'Amico, F. Pomponi and J. Hart, *J. Clean. Prod.*, 2021, **279**, 123487.
4 A. I. Bartlett, R. M. Hadden and L. A. Bisby, *Fire Technol.*, 2019, **55**, 1–49.
5 C. Pettersson, Fire safety in timber buildings - A review of existing knowledge, *Bradforsk Rep.*, 2020, **10**, 81.
6 R. Gerard, D. Barber and A. Wolski, Fire Safety Challenges of Tall Wood Buildings, Phase 1: Final Report, Dec 6, 2013. Fire Protection Research Foundation of the National Fire Protection Association (NFPA). Arup North America Ltd. One Batterymarch Park, Quincy, Massachusetts, USA.
7 B. Phillip, *Nature*, 2020, **577**, 153–154.
8 S. L. Zelinka, M. Altgen, L. Emmerich, N. Guigo, T. Keplinger, M. Kymäläinen, E. E. Thybring and L. G. Thygesen, *Forests*, 2022, **13**, 1004.
9 D. Sandberg, A. Kutnar and G. Mantanis, *iForest*, 2017, **10**, 895–908.
10 E. I. Akpan, B. Wetzel and K. Friedrich, *Green Chem.*, 2021, **23**, 2198–2232.
11 K. Candelier, M.-F. Thevenon, A. Petrissans, S. Dumarcay, P. Gerardin and M. Petrissans, *Ann. For. Sci.*, 2016, **73**, 571–583.
12 D. Jones and D. Sandberg, in Procedings of COST Action FP1407 WG1 and WG4 meeting. *Wood modification in Europe: processes, products, applications*. ed. Goli G. and Todaro L. Firenze, Italy, 26th February, 2018.
13 Flame Retardant Chemicals: Technologies and Global Markets BCC Research, Report Overview, CHM014R, 2025.
14 C.-M. Popescu and A. Pfriem, *Fire Mater.*, 2019, **44**(1), 100–111.
15 M. Dogan, S. D. Dogan, L. A. Savas, G. Ozcelik and U. Tayfun, *Composites, Part B*, 2021, **222**, 109088.
16 L. A. Lowden and T. R. Hull, *Fire Sci. Rev.*, 2013, **2**, 4.
17 D. N. Obanda, T. F. Shupe and H. M. Barnes, *Bioresour. Technol.*, 2008, **99**, 7312–7322.
18 P. Sauerbier, A. K. Mayer, L. Emmerich and H. Militz, *Fire Retardant Treatment of Wood - State of the Art and Future Perspectives*. Internatinal Conference Wood & Fire Safety. ed. L. Makovicka Osvaldova, F. Markert, S. L. Zelinka, 2020. 97–102.
19 R. Regulation, https://echa.europa.eu/candidate-list-table, 2010.
20 N. Hadrup, M. Frederiksen and A. K. Sharma, *Regul. Toxicol. Pharmacol.*, 2021, **121**, 104873.
21 A. B. Morgan and M. Kilinc, *Non-Halogenated Flame Retardant Handbook*, 2021, pp. 271–308, DOI: 10.1002/9781119752240.ch6.
22 T. Kashiwagi, J. W. Gilman, K. M. Butler, R. H. Harris, J. R. Shields and A. Asano, *Fire Mater.*, 2000, **24**, 277–289.
23 A. M. Pereyra and C. A. Giudice, *Fire Saf. J.*, 2009, **44**, 497–503.
24 E. Garskaite, O. Karlsson, Z. Stankeviciute, A. Kareiva, D. Jones and D. Sandberg, *RSC Adv.*, 2019, **9**, 27973–27986.
25 M. Matinfar and J. A. Nychka, *Adv. Colloid Interface Sci.*, 2023, **322**, 103036.
26 T. Skorina and I. Tikhomirova, *J. Mater. Sci.*, 2012, **47**, 5050–5059.

27 B. Neyses, L. Rautkari, A. Yamamoto and D. Sandberg, *iForest*, 2017, **10**, 857–864.
28 G. B. Alexander, W. M. Heston and R. K. Iler, *J. Phys. Chem.*, 1954, **58**, 453–455.
29 H. H. Weldes and K. R. Lange, *Ind. Eng. Chem.*, 1969, **61**, 29–44.
30 C. Mai and H. Militz, *Wood Sci. Technol.*, 2004, **37**, 339–348.
31 D. Dimas, I. Giannopoulou and D. Panias, *J. Mater. Sci.*, 2009, **44**, 3719–3730.
32 R. Iler and P. Pinkney, *Ind. Eng. Chem.*, 1947, **39**, 1379–1384.
33 Y. Ma, P. Li, Y. Zuo, Y. Zhang, J. Qiao and Y. Wu, *Ind. Crop, Prod.*, 2025, **233**, 121443.
34 B. Neyses, L. Rautkari, A. Yamamoto and D. Sandberg, *iForest*, 2017, **10**, 857–864.
35 V. Merk, M. Chanana, T. Keplinger, S. Gaan and I. Burgert, *Green Chem.*, 2015, **17**, 1423–1428.
36 H. Choi, L. E. Dalton, I. Peszlen and M. Pourghaz, *Composites, Part B*, 2024, **275**, 111324.
37 H. Guo, M. Özparpucu, E. Windeisen-Holzhauser, C. M. Schlepütz, E. Quadranti, S. Gaan, C. Dreimol and I. Burgert, *ACS Sust. Chem. Eng.*, 2020, **8**, 10402–10412.
38 E. Garskaite, G. Balciunas, M. Drienovsky, D. Sokol, D. Sandberg, A. C. Bastos and A. N. Salak, *RSC Adv.*, 2023, **13**, 5813–5825.
39 D. Kocaefe, X. Huang and Y. Kocaefe, *Curr. For. Rep.*, 2015, **1**, 151–161.
40 H. Sreenivasan, E. Bernard, H. S. Santos, H. Nguyen, S. Moukannaa, A. Adediran, J. L. Provis and P. Kinnunen, *Cem. Concr. Res.*, 2024, **178**, 107462.
41 M. Sambucci, A. Sibai and M. Valente, *J. Compos. Sci.*, 2021, **5**, 109.
42 M. J. Timoney, B. A. McCabe and A. L. Bell, Experiences in dry soil mixing in highly organic soils in Proceedings of the Institution of Civil Engineers – Ground Improvement, 2012, **165**, 3–14.
43 J. L. Bañuelos, E. Borguet, G. E. Brown, Jr., R. T. Cygan, J. J. DeYoreo, P. M. Dove, M.-P. Gaigeot, F. M. Geiger, J. M. Gibbs, V. H. Grassian, A. G. Ilgen, Y.-S. Jun, N. Kabengi, L. Katz, J. D. Kubicki, J. Lützenkirchen, C. V. Putnis, R. C. Remsing, K. M. Rosso, G. Rother, M. Sulpizi, M. Villalobos and H. Zhang, *Chem. Rev.*, 2023, **123**, 6413–6544.
44 R. A. Youness, D. M. Tag El-deen and M. A. Taha, *Silicon*, 2023, **15**, 2493–2505.
45 F. P. Byrne, S. Jin, G. Paggiola, T. H. M. Petchey, J. H. Clark, T. J. Farmer, A. J. Hunt, C. Robert McElroy and J. Sherwood, *Sustain. Chem. Process.*, 2016, **4**, 7.
46 I. L. Svensson, S. Sjöberg and L.-O. Öhman, *J. Chem. Soc., Faraday Trans. 1*, 1986, **82**, 3635–3646.
47 M. R. Marsiske, R. Köser, B. Bäumle and C. Ruiz-Agudo, *ACS Appl. Eng. Mater.*, 2023, **1**, 696–707.
48 M. Kley, A. Kempter, V. Boyko and K. Huber, *Langmuir*, 2017, **33**, 6071–6083.
49 W. L. Marshall and J. M. Warakomski, *Geochim. Cosmochim. Acta*, 1980, **44**, 915–924.
50 D. Prasad and N. Mitra, *Phys. Chem. Chem. Phys.*, 2022, **24**, 21308–21320.
51 R. K. Iler, *The chemistry of silica: Solubility, polymerization, colloid and surface properties, and biochemistry*, Wiley, New York, 1979.
52 D. A. Sverjensky, *Geochim. Cosmochim. Acta*, 2005, **69**, 225–257.
53 Y. Zhong, J. Li, H. Wang and M. Wang, *Mater. Chem. Phys.*, 2025, **337**, 130613.
54 M. Steiger, K. Linnow, D. Ehrhardt and M. Rohde, *Geochim. Cosmochim. Acta*, 2011, **75**, 3600–3626.
55 D. Nied, K. Enemark-Rasmussen, E. L'Hopital, J. Skibsted and B. Lothenbach, *Cem. Concr. Res.*, 2016, **79**, 323–332.
56 E. Bernard, H. Nguyen, S. Kawashima, B. Lothenbach, H. Manzano, J. Provis, A. Scott, C. Unluer, F. Winnefeld and P. Kinnunen, *RILEM Tech. Lett.*, 2023, **8**, 65–78.
57 T. Runčevski, C. Wu, H. Yu, B. Yang and R. E. Dinnebier, *J. Am. Ceram. Soc.*, 2013, **96**, 3609–3616.
58 S. A. Walling and J. L. Provis, *Chem. Rev.*, 2016, **116**, 4170–4204.
59 E. Gartner and T. Sui, *Cem. Concr. Res.*, 2018, **114**, 27–39.
60 Q. Song, J. Su, J. Nie, H. Li, Y. Hu, Y. Chen, R. Li and Y. Deng, *Constr. Build. Mater.*, 2021, **293**, 123494.
61 S. A. Bernal, J. L. Provis, R. J. Myers, R. San Nicolas and J. S. J. van Deventer, *Mater. Struct.*, 2015, **48**, 517–529.
62 A. Leemann, B. Münch, B. Lothenbach, E. Bernard, C. Trottier, F. Winnefeld and L. Sanchez, *Cem. Concr. Res.*, 2025, 195.
63 F. Zunino and K. Scrivener, *Cem. Concr. Res.*, 2022, **160**, 106930.
64 M. Tonelli, F. Martini, L. Calucci, E. Fratini, M. Geppi, F. Ridi, S. Borsacchi and P. Baglioni, *Dalton Trans.*, 2016, **45**, 3294–3304.
65 R. Snellings, P. Suraneni and J. Skibsted, *Cem. Concr. Res.*, 2023, **171**, 107199.
66 M. H. Ramage, H. Burridge, M. Busse-Wicher, G. Fereday, T. Reynolds, D. U. Shah, G. Wu, L. Yu, P. Fleming, D. Densley-Tingley, J. Allwood, P. Dupree, P. F. Linden and O. Scherman, *Renew. Sustain. Energy Rev.*, 2017, **68**, 333–359.
67 P. Evans, Weathering and Photoprotection of Wood, *In Development of Commercial Wood Preservatives*, 2008.
68 L. Hansson, J. Couceiro and B.-A. Fjellner, *Wood Mater.Sci. Eng.*, 2017, **12**, 251–256.
69 R. Golubevas, Z. Stankeviciute, A. Zarkov, R. Golubevas, L. Hansson, R. Raudonis, A. Kareiva and E. Garskaite, *Mater. Adv.*, 2020, **1**, 1675–1684.
70 M. F. Ashby and D. R. H. Jones, in *Engineering Materials 2*, ed. M. F. Ashby and D. R. H. Jones, Butterworth-Heinemann, Boston, 2013, 4th edn, pp. 493–508, DOI: 10.1016/B978-0-08-096668-7.00029-2.
71 L. André, N. Devau, P. Pedenaud and M. Azaroual, *Procedia Earth Planet. Sci.*, 2017, **17**, 217–220.
72 A. Spinthaki, G. Petratos, J. Matheis, W. Hater and K. D. Demadis, *Geothermics*, 2018, **74**, 172–180.
73 E. Garskaite, S. L. Stoll, F. Forsberg, H. Lycksam, Z. Stankeviciute, A. Kareiva, A. Quintana, C. J. Jensen,

K. Liu and D. Sandberg, *ACS Omega*, 2021, **6**(33), 21719–21729.
74 M. Schwanninger, J. C. Rodrigues, H. Pereira and B. Hinterstoisser, *Vib. Spectr.*, 2004, **36**, 23–40.
75 C. Namyslo Jan, E. Kaufmann Dieter, C. Mai and H. Militz, *Holzforschung*, 2015, **69**, 595.
76 Ö. Özgenç, S. Durmaz, I. H. Boyaci and H. Eksi-Kocak, *Spectrochim. Acta, Part A*, 2017, **171**, 395–400.
77 R. Evans, H. Newman Roger, C. Roick Ute, D. Suckling Ian and F. A. Wallis Adrian, *Holzforschung*, 1995, **49**, 498.
78 M. Altgen, M. Awais, D. Altgen, S. Kyyrö, H. Seppäläinen and L. Rautkari, *J. Mater. Sci.*, 2020, **55**, 12621–12635.
79 L. Vidal, E. Joussein, M. Colas, J. Cornette, J. Sanz, I. Sobrados, J. L. Gelet, J. Absi and S. Rossignol, *Colloids Surf., A*, 2016, **503**, 101–109.
80 J. Davis and P. Wells, *Ind. Metrol.*, 1992, **2**, 195–218.
81 J. Couceiro, O. Lindgren, L. Hansson, O. Söderström and D. Sandberg, *Wood Mater. Sci. Eng.*, 2019, **14**, 437–444.
82 Z. Fu, J. Chen, Y. Zhang, F. Xie and Y. Lu, *Polymers*, 2023, **15**, 3295.
83 S. V. Glass, N. Farkas, S. L. Zelinka, G. Finch and N. Helbach, *A Conceptual Approach for Developing Guidelines to Prevent Drying Cracks in Mass Timber*, ed. U. Berardi, Springer Nature, Singapore, 2025, IABP 2024, LNCE 552, pp. 276–283.
84 D. Elustondo, N. Matan, T. Langrish and S. Pang, *Dry. Technol.*, 2023, 41, 890–914.
85 P. Tian, H. Qiu and H. Wang, *J. Buil. Eng.*, 2021, **44**, 102632.
86 K. D. Demadis, A. Ketsetzi and E.-M. Sarigiannidou, *Ind. Eng. Chem. Res.*, 2012, **51**, 9032–9040.
87 R. K. Iler, Colloidal Components in Solutions of Sodium Silicate, *Soluble Silicates*, American Chemical Society, 1982, vol. 194, ch. 7, pp. 95–114.
88 J. Schott, O. S. Pokrovsky and E. H. Oelkers, *Rev. Mineral. Geochem.*, 2009, **70**, 207–258.
89 S. Altun, A. Ozcıfcı, A. Senel, E. Baysal and H. Toker, *Wood Res.*, 2010, **55**, 101–112.
90 E. Garskaite, *et al.*, Development of sustainable fire retardants for increased usage of wood in the built environment SWECO report, 2025, 38.
91 L. S. Dent Glasser and C. K. Lee, *J. Appl. Chem. Biotechnol.*, 1971, **21**, 127–133.
92 H. Roggendorf, D. Böschel and J. Trempler, *J. Non-Cryst. Solids*, 2001, **293–295**, 752–757.
93 A. Pfeffer, C. Mai and H. Militz, *Eur. J. Wood Prod.*, 2012, **70**, 165–176.
94 I. Halasz, M. Agarwal, R. Li and N. Miller, *Catal. Lett.*, 2007, **117**, 34–42.
95 O. Yarema, M. Yarema and V. Wood, *Chem. Mater.*, 2018, **30**, 1446–1461.
96 C. Jäger, J. Dorschner, H. Mutschke, T. Posch and T. Henning, *A&A*, 2003, **408**, 193–204.
97 L. Dalstein, E. Potapova and E. Tyrode, *Phy. Chem. Chem. Phys.*, 2017, **19**, 10343–10349.
98 R. C. Longo, F. Königer, A. Nefedov and P. Thissen, *ACS Sust. Chem. Eng.*, 2019, **7**, 8449–8457.
99 H. Cho, A. R. Felmy, R. Craciun, J. P. Keenum, N. Shah and D. A. Dixon, *J. Am. Chem. Soc.*, 2006, **128**, 2324–2335.
100 E. Garskaite, *et al.*, In-situ synthesis of calcium phosphates derived from eggshells to improve wood reaction-to-fire properties, *Brandforsk Rep.*, 2022, **7**, 50.